# Hydrogen-Bonded Networks Along and Bifurcation of the E-Pathway in Quinol:Fumarate Reductase

Elena Herzog,[†‡Δ] Wei Gu,[§Δ] Hanno D. Juhnke,[†] Alexander H. Haas,[†] Werner Mäntele,[¶] Jörg Simon,[||] Volkhard Helms,[§*] and C. Roy D. Lancaster[†‡*]

[†]Department of Molecular Membrane Biology, Max Planck Institute of Biophysics, Frankfurt am Main, Germany; [‡]Department of Structural Biology, Center of Human and Molecular Biology, Institute of Biophysics, Faculty of Medicine, Saarland University, Homburg, Germany; [§]Center for Bioinformatics and Center of Human and Molecular Biology, Saarland University, Saarbrücken, Germany; and [¶]Institute of Biophysics and [||]Institute of Molecular Biosciences, J. W. Goethe University, Frankfurt am Main, Germany

ABSTRACT The E-pathway of transmembrane proton transfer has been demonstrated previously to be essential for catalysis by the diheme-containing quinol:fumarate reductase (QFR) of *Wolinella succinogenes*. Two constituents of this pathway, Glu-C180 and heme $b_D$ ring C ($b_D$-C-) propionate, have been validated experimentally. Here, we identify further constituents of the E-pathway by analysis of molecular dynamics simulations. The redox state of heme groups has a crucial effect on the connectivity patterns of mobile internal water molecules that can transiently support proton transfer from the $b_D$-C-propionate to Glu-C180. The short H-bonding paths formed in the reduced states can lead to high proton conduction rates and thus provide a plausible explanation for the required opening of the E-pathway in reduced QFR. We found evidence that the $b_D$-C-propionate group is the previously postulated branching point connecting proton transfer to the E-pathway from the quinol-oxidation site via interactions with the heme $b_D$ ligand His-C44. An essential functional role of His-C44 is supported experimentally by site-directed mutagenesis resulting in its replacement with Glu. Although the H44E variant enzyme retains both heme groups, it is unable to catalyze quinol oxidation. All results obtained are relevant to the QFR enzymes from the human pathogens *Campylobacter jejuni* and *Helicobacter pylori*.

## INTRODUCTION

The membrane protein complex quinol:fumarate reductase (QFR) is the terminal enzyme of anaerobic fumarate respiration that allows bacteria to use fumarate as the terminal electron acceptor (1,2). QFR couples the two-electron reduction of fumarate to succinate to the two-electron oxidation of quinol to quinone. The QFR enzymes of the $\varepsilon$-proteobacteria *Wolinella succinogenes*, *Helicobacter pylori*, and *Campylobacter jejuni* (3,4) are homodimeric complexes of heterotrimers of A, B, and C subunits. Each heterotrimer contains two heme *b* groups bound by the transmembrane subunit C, which are termed the proximal heme, $b_P$, and the distal heme, $b_D$, according to the relative proximity to the hydrophilic subunits A and B (5). The three-dimensional structure of the QFR from *W. succinogenes* has been determined by x-ray crystallography, initially at a resolution of 2.2 Å (5), which was later improved to 1.78 Å (6). The site of fumarate reduction has been shown (5,7) to be located in subunit A, close to the isoalloxazine ring of the flavin adenine dinucleotide (FAD, Fig. 1 *a*). The site of menaquinol oxidation is located close to heme $b_D$ in a cavity lined by a number of residues including, in particular, His-C44 (a heme $b_D$ ligand, with C denoting the C subunit) and Glu-C66. The latter side chain has previously been demonstrated to be selectively essential for menaquinol oxidation (8).

Electron transfer via the two heme groups has been proposed (9) and demonstrated (6) to be coupled to a compensatory, parallel transfer of one proton per electron via a transmembrane proton transfer pathway, which is transiently open during the reduction of the heme groups and blocked in the oxidized state of the enzyme (9). The two most prominent constituents of the proposed pathway were suggested to be the heme $b_D$ ring C ($b_D$-C-) propionate and the side chain of amino acid residue Glu-C180, after which the proton transfer pathway was named the "E-pathway" (9) (Fig. 1 *b*). The essential role of Glu-C180 was supported by site-directed mutagenesis and structural and functional characterization of the enzyme E180Q, where the Glu-C180 was replaced with a Gln residue (10). Moreover, multiconformer continuum electrostatics (MCCE) calculations (11) and Fourier-transform infrared (FTIR) spectroscopy experiments (12) indicated that the Glu-C180 side chain undergoes a combination of

*Submitted September 13, 2011, and accepted for publication July 25, 2012.*

[Δ]Elena Herzog and Wei Gu contributed equally to this work.

*Correspondence: volkhard.helms@bioinformatik.uni-saarland.de or roy.lancaster@structural-biology.eu

Wei Gu's present address is Saarland University Hospital, Clinic for Psychiatry and Psychotherapy, Homburg, Germany.

Hanno D. Juhnke's present address is Sanofi-Aventis Deutschland GmbH, Site Frankfurt Devices, Frankfurt am Main, Germany.

Alexander H. Haas's present address is Forschungszentrum Jülich GmbH, Jülich, Germany.

Jörg Simon's present address is Fachbereich Biologie, Technische Universität Darmstadt, Darmstadt, Germany.



Editor: Leonid Brown.



0006-3495/12/09/1305/10 $2.00

http://dx.doi.org/10.1016/j.bpj.2012.07.037

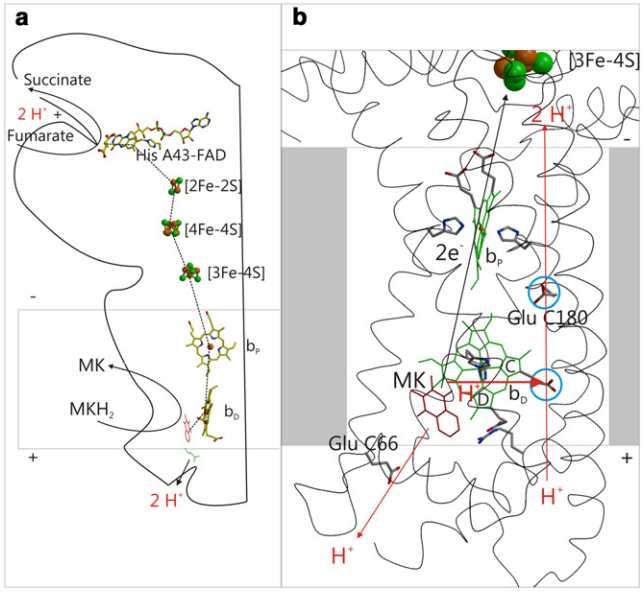


FIGURE 1 Modified E-pathway hypothesis and the electron and proton transfer in the *Wolinella succinogenes* QFR (9,15). (*a*) The prosthetic groups of one of the two heterotrimeric complexes of the QFR homodimer are shown, as are the locations of the binding sites for fumarate and menaquinol ($MKH_2$). The arrangement of the prosthetic groups, such as heme $b_D$, heme $b_P$, [3Fe-4S], [4Fe-4S], [2Fe-2S], and FAD, indicates that electron transfer from the site of menaquinol oxidation to the site of fumarate reduction proceeds via the six prosthetic groups of one monomer in the homodimer. (*b*) Transfer of electrons and protons is shown. Two protons are liberated upon menaquinol ($MKH_2$) oxidation and two protons are transferred via the ring C-propionate of the distal heme (heme $b_D$) and the Glu-C180 to the cytoplasm to make the overall reaction electroneutral. In the oxidized state of the enzyme, the E-pathway is blocked. However, upon reduction, the E-pathway is open.

a conformational change and protonation upon heme reduction. The contribution of the $b_D$-C-propionate is supported by a combination of $^{13}C$ labeling of the heme propionates and redox-induced FTIR experiments (13), indicating a change in protonation, possibly accompanied by a change in environment upon heme reduction. More recent experimental evidence (14) indicates that the two E-pathway protons have different points of entry, with one being taken up from the periplasmic surface and the other possibly being provided directly by quinol oxidation (Fig. 1 *b*) (14,15). However, it has not been clear on the basis of the available crystal structure of the oxidized enzyme how proton transfer could occur between the quinol oxidation site and the E-pathway. In addition, although the $b_D$-C-propionate and Glu-C180 were identified as the most prominent components of the proton transfer pathway, it has also not been clear, on the basis of the structure, how proton transfer could occur between them. Furthermore, two constituents are not enough to span the membrane region, and the additional participants in the proton-transfer pathway must be identified.

All available crystal structures of the QFR are those of the oxidized enzyme. However, functionality of the E-pathway requires the enzyme to be reduced (9). Lacking an experimentally determined structure of the reduced enzyme, it is advantageous to perform computer simulations of various redox states of the enzyme to determine, for instance, how the side chain of Glu-C180 and the $b_D$-C-propionate react to changes of the redox states of the heme groups and why the E-pathway is blocked in the oxidized state of the enzyme.

Since an atomistic investigation of proton transfer in this system is not yet possible experimentally, classical molecular dynamics (MD) simulation is an appropriate theoretical method (16–18) to investigate the postulated mechanism of electron-coupled proton transfer in QFR. The advantage of the MD simulations over the experiments and the continuum electrostatics calculations performed so far is that they allow the analysis of time-dependent properties. In particular, the conformational behavior of various residues and their side chains and any environmental changes may be directly observed during MD simulations. Whereas classical MD simulations cannot be used to study proton-transfer reactions directly, because they generally do not incorporate bond-breaking phenomena (19,20), they can provide information on the formation of configurations that would allow either direct proton transfer between donor and acceptor residues or indirect proton transfer mediated by water molecules. By analyzing changes in hydrogen-bonded networks during MD simulations, one can propose configurations that would enable proton-transfer events. Friedman and co-workers studied proton transfer between adjacent carboxylate groups on the protein surface of the ribosomal protein S10 using classical MD simulations (19). Their results demonstrate that random fluctuations of the residues on the surface occasionally lead to configurations where carboxylates either share a common proton through a hydrogen bond or are connected by a few water molecules forming potentially conducting networks (19). In the area of proton-conducting membrane proteins, similar studies have addressed the formation of hydrogen-bonded networks, for example, in cytochrome *c* oxidase (21–24) and in bacteriorhodopsin (25,26). On the other hand, the establishment of proton-conducting networks, especially inside membrane-bound proteins, may also be a rare event. This could mean that these would only form infrequently and may not be observable on the timescale of MD simulations, or that they would only form in the presence of the explicit proton.

Three-dimensional structures of proteins determined by x-ray and/or neutron diffraction methods provide average positions occupied in the crystal of well-ordered or bound water molecules (27,28). Water molecules that show weak electron density are typically not included in the final structure due to the limitations of the crystallographic model refinement (29,30). Therefore, atomic coordinates of less ordered bound waters, waters that interact with protein surface, or bulk waters may not be identified (for review, see Karplus and Faerman (27) and Meyer (31)). These limitations leave protein structures with cavities that should be

filled with water molecules, if these water molecules can experience sufficient favorable interactions with polar protein groups or other water molecules. It is thus standard practice (see, e.g., Huang and Tajkhorshid (32) and Holyoake and Sansom (33)) to fill such polar protein cavities with water before starting MD simulations. A number of theoretical methods exist to identify interior cavities of macromolecules by analyzing protein structures (34). The majority of these methods are based on the concept of solvent-accessible (35) or molecular-contact surfaces (36), which are obtained by rolling a spherical probe over the molecule (37).

Since interactions of water molecules with proteins play an important role in protein structure, dynamics, and function (38), we used one of the theoretical methods, GRID, developed by Goodford (39), to search for cavities in the QFR and fill them with additional water molecules not identified crystallographically. This strategy was previously used successfully on various other soluble and membrane protein systems (21,40,41). Subsequently, MD simulations were performed on five redox states of the QFR, allowing identification of hydrogen-bonded networks formed by donor/acceptor residues and internal water molecules in this enzyme.

Here, we present computational results supporting the functional role of buried water molecules in the transient proton transfer from $b_D$-C-propionate to Glu-180, the two important constituents in the E-pathway identified experimentally. The simulations provide the formation of continuous H-bonded pathways by these buried water molecules as a mechanistic explanation for the opening of the E-pathway in the reduced state of the enzyme. In addition, the heme $b_D$ ligand, His-C44, also was found to form H-bonds with the $b_D$-C-propionate, suggesting its functional role in the proton transfer. A functionally essential role of His-C44 is demonstrated by site-directed mutagenesis and characterization of the variant enzyme.

## MATERIALS AND METHODS

Mutagenesis, cell growth, purification of QFR, and spectroelectrochemical redox titrations are described in the Supporting Material, as is the construction of the atomic model. As in PDB entry 2BS3, the second set of subunits A, B, and C in the homodimer are referred to as D, E, and F, respectively. Also described is the preparation of five different redox states for MD simulations (Fig. S1, Fig. S2, and Table S1 in the Supporting Material). Briefly, these redox states are termed A (fully oxidized, $b_D$-C-propionate-protonated, Glu-C/F180-deprotonated), A′ (fully oxidized, $b_D$-C-propionate-deprotonated, Glu-C/F180-deprotonated), B (semireduced, $b_D$-C-propionate-protonated, Glu-C/F180-protonated), C (fully reduced, $b_D$-C-propionate-protonated, Glu-C/F180-protonated), and C′ (fully reduced, $b_D$-C-propionate-deprotonated, Glu-C/F180-protonated).

### Computational determination of water-binding sites

The program GRID (39) was used to find water-binding sites in QFR. GRID provides a method to detect energetically favorable binding sites for functional groups on molecules of known structure. In the past, different binding energetic criteria have been used to position water molecules in protein cavities (42). For example, the DOWSER program (43) was used to place water molecules in the cavities of the cytochrome *c* oxidase with chemical potential in the range −10 to −5 kcal/mol (44). An upper threshold of −6 kcal/mol was suggested in a study (45) of the cytochrome P450cam using the GRID (39) program. Using much more extended sampling and a semi-grand-canonical treatment of the waters in the protein cavity, the same system has been reinvestigated (46) with essentially the same result for the occupancy of unliganded and camphor-bound cytochrome p450cam as reported earlier (47,48). A grid spacing of 1 Å was used in this study for the water-probe scan. In total, 78 buried water molecules constituted the initial model system for MD simulation; of these water molecules, 54 were modeled waters with GRID energies $\leq -6.0$ kcal/mol and 24 were crystallographically defined water molecules (see Fig. S3 and Table S2).

### MD simulations

The simulation system included the membrane subunit dimer, consisting of the C and F membrane subunits. The system was first inserted into a DOPC lipid bilayer membrane (49) and was then solvated using the SPC/E water model (50). The simulation box had a size of 97 × 98 × 98 Å$^3$ (Fig. S4). 10 - 14 counterions were added depending on the redox state to neutralize the system. The GROMACS package (version 4.0.4) (51) was used to propagate Newton's equations of motion. Protein atoms and water molecules were treated according to the AMBER 99 force field (52), and GAFF parameterization (49) was used for the lipid molecules. The LINCS procedure (53) was applied to constrain all bond lengths. A 10-Å cutoff was used for the short-range nonbonded interactions and the lists of nonbonded pairs were updated every 10 steps. The particle-mesh Ewald (PME) method (54) with a grid size of 1.2 Å was used to calculate long-range electrostatic interactions. The system temperature (300 K) was maintained by weak coupling to an external bath in the simulations (55). The system was first equilibrated during 1 ns of MD in the NPT ensemble with semi-isotropic pressure coupling that separates the coupling in the *xy* dimension (along the membrane surface) and in the *z* dimension (along the membrane normal). The reference pressure, compressibility, and time constant for coupling were set to 1 bar, $4.5 \times 10^{-5}$ bar$^{-1}$, and 1 ps, respectively. Then, for each of the five states, A, A′, C, C′, and B, two simulations of 30-ns length were performed in the NVT ensemble. The two sets of repeat runs were each started from different conformations after equilibration. The time step of the simulation was set to 2 fs. The total simulation length of the data-collecting runs is 300 ns.

### Analysis of hydrogen-bonded networks

We performed detailed analyses of the hydrogen bond network between Glu-C/F180 and heme $b_D$ for the five different redox and protonation states of the protein. (see also Supporting Material) First, we identified connected hydrogen-bonding paths (HBPs) extending from Glu-C/F180 to the corresponding heme $b_D$ groups. Then, using the Dijkstra algorithm by giving identical weights to all hydrogen bonds, we measured the lengths of these paths by the minimum number of hydrogen bonds between the source and destination. The distribution of the lengths of all HBPs over the simulation time are of higher relevance to the proton-conducting process than the overall frequency of finding an HBP and the average length of these paths. This is because the proton-conducting rate for proton transfer, especially that for concerted proton transfer, has been described as decreasing exponentially with the distance between the source and the sink (56–58). Therefore, the proton-conducting rate is largely determined by the number of short HBPs instead of the frequency (number) of all HBPs. Here, we applied a rather strict definition of hydrogen bond length, $d_{OW-OW} \leq 2.75$ Å and $d_{O\delta-OW} \leq 3.00$ Å, identified as tight enough for productive proton transfer

in previous Q-HOP MD simulations allowing for explicit proton-transfer events (59).

## RESULTS AND DISCUSSION

### Analyses of the trajectories from the MD simulations

The stored conformations were analyzed by means of root mean-square deviations (RMSDs) compared to the minimized starting structure and by root mean-square fluctuations (RMSFs, see Fig. S5, Fig. S6, and Fig. S7). After 10 ns, all RMSDs appear to fluctuate around values of 0.15–0.25 nm, which are typical values observed in MD simulations of stably folded soluble or transmembrane proteins of this size. The solvent-exposed loops were significantly more flexible than the transmembrane parts (Fig. S7). However, those fluctuations of the soluble elements are not expected to be relevant to the questions we are studying. We also performed an all-to-all analysis of the $C_\alpha$ RMSD (Fig. S8), as suggested by Grossfield and Zuckerman (60). We do not detect signs for structural drifts during the simulations. Together with the observation of frequent forming and breaking of the hydrogen-bonding network (see below), we believe that our simulations have reached the relative equilibration that is required for a statistically meaningful analysis of molecular simulations. In particular, the relevant structures of the protein in all simulations were stable and sufficiently well equilibrated for the purpose of analyzing the dynamics of water wires in the buried E-pathway. The key residues Glu-C/F180 and His-C/F44 showed very small RMS fluctuations, meaning that their backbone structure hardly changed among the five different states. Although some catalysis-related conformational changes are inferred from FTIR experiments (12), these could be accounted for mainly by the opening and closing of the capping domain in subunit A (7), which is not within the scope of this study. The finding of only small backbone fluctuations in the regions of interest here is in contrast to the importance of the structural transitions of the side chains of the residues identified in this work that are postulated to play an important role in proton transfer in QFR (see below).

### Hydrogen-bonded networks between the $b_D$-C-propionate and Glu-180

Since proton transfer involves either titratable residues and/or water molecules, the H-bonded network provided by buried water molecules between the $b_D$-C-propionate and Glu-C/F180 appears crucial for the proton transfer along the E-pathway. We observed that the distances between heme $b_D$ and Glu-C/F180 showed large fluctuations (see Fig. 2, *a* and *b*). At distances <0.83 nm (the distance in the x-ray structure), the two groups were always connected via bridging water molecules. At distances >0.83 nm, we observed conformations with or without connecting long hydrogen-bonding pathways (including at least four hydrogen bonds). Fig. 2 *c* illustrates that the overall protein structure, as well as that of heme $b_D$, remained almost unchanged, and the transitions between short and long distances were apparently linked to a conformational change of the Glu-C/F180 side chains (Fig. 2, *e* and *f*). The side-chain conformations observed are consistent with the predictions from multiconformation continuum electrostatics calculations (11) and with the 1.78-Å-resolution crystal structure (PDB entry 2BS2 (6); Fig. S9). The restriction of the conformational transition to the Glu side chains is also in agreement with the RMSF analysis showing small fluctuations for the Glu-C/F180 backbone. Switching between alternate conformations of Glu-C/F180 may occur spontaneously on timescales of 10 ns and longer (Fig. S10 and Fig. S11). The lengths of HBPs in each simulation, as well as the distribution of their lengths, are shown in Fig. 3. Clearly, many more short HBPs were observed in the reduced states, C and C′, especially for the deprotonated-reduced state C′. Similar results were found in the repeat runs (see Fig. S12).

To quantify the contributions of all HBPs found in the simulation of each state, we computed a pseudo proton conductance, $G^*$, of each simulation that can be assumed as proportional to the real conductance, $G$. $G^*$ was defined as

$$G^* = \sum_i \alpha^{L_i - 1}, \tag{1}$$

where $L_i$ is the length of $HBP_i$, $\alpha$ ($0 < \alpha < 1$) represents the dependence of the conductance on the length of the HBP, and the summation runs over all 10-ps-spaced snapshots in a window of a given length. When $L_i = 1$, a direct hydrogen bond is formed between the source and the sink and therefore, the conductance does not depend on $\alpha$. The parameter $\alpha$ likely depends on the nature of a particular reaction system. Therefore, its exact value is unknown in the present case. For several chromophoric molecules, $\alpha$ has been estimated by fitting the proton transfer rates to experimental measurements (56). This gave $\alpha$ values in the range $10^{-2}$ to $10^{-3}$ for different temperatures. For such small values of $\alpha$, states with more short HBPs, such as state C′, will obviously have a much larger proton conductance according to Eq. 1. Compared to the results of Cox et al. (56), the $\alpha$ values of 0.1 and 0.5 used here can be termed rather permissive. However, the $\alpha$ value of 0.2 determined in other studies (57,58) falls right in between the two values we have used. $G^*$ was computed using a sliding window of 1 ns for all simulations (Fig. 2, *g* and *h*). We also computed an accumulated $G^*$ (Fig. 2, *i* and *j*). Even with $\alpha = 0.5$, the conductance and accumulated conductance of states C and C′ were much larger than for the other states in both monomers (Fig. 2, *g–j*). As expected, this effect was even stronger for $\alpha = 0.1$ (Fig. S13). When

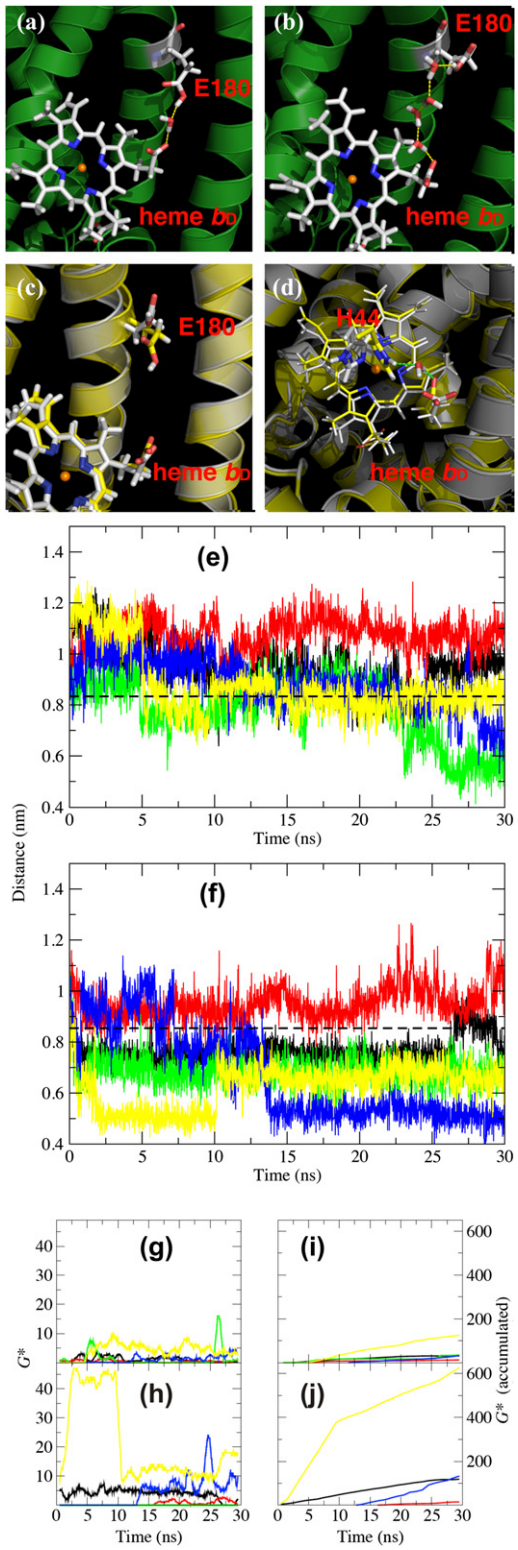


FIGURE 2 MD snapshots of the (*a*) shorter hydrogen-bonded path between Glu-C/F180 and heme $b_{D,}$ (*b*) longer hydrogen-bonded path. (*c*) Superposition of an MD snapshot with longer Glu-C/F180-to-heme-$b_D$ distance (*white helix and carbon atoms*) and one with shorter corresponding distance (*yellow helix and carbon atoms*). The structural reason for the shorter distance, i.e., a shorter path resulting in larger proton conductance (see Fig. 2, *e* and *f*), is a flipping of the side chain of Glu-C/F180. (*d*) Superposition of an MD snapshot without HBPs (*white helix and carbon atoms*) and one with HBPs formed (yellow helix and carbon atoms) between His C/F 44 and heme $b_D$. Side chains of His-C/F44, a bridging water molecule, as well as the carboxyl group of heme $b_D$, are highlighted by using thicker sticks. (*e* and *f*) Minimum distances between the carboxyl groups of Glu-C/F180 and heme $b_D$ during the simulations of different states A (*black*), A′ (*red* ), B (*green*), C (*blue*), and C′ (*yellow*) for monomers C (*e*) and F (*f*). Dashed lines show the value in the starting structures. (*g–j*) Pseudoconductance, $G^*$, during the simulations using $\alpha = 0.5$ (*g* and *h*) and accumulated $G^*$ using $\alpha = 0.5$ (*i* and *j*) for path C (*g* and *i*) and path F (*h* and *j*). Coloring coding of the five redox states is the same as for *e* and *f*.

assuming small values of $\alpha$ in the range $10^{-2}$ to $10^{-3}$, as found in Cox et al. (56), only the reduced states can conduct protons from a kinetic point of view. Some large values of $G^*$ were also found in the Glu-C180 path of state B. This is due to short HBPs formed occasionally during the simulation. In the repeat run, as well as when extending the simulation to 40 ns, this phenomenon was not observed (Fig. S14). This indicates that short HBPs form only rarely in state B compared to states C and C′. These results correlate with the experimental observation that the E-pathway is only opened in the (semi-)reduced states (6,10). Thus, we suggest that the frequently formed short HBPs in the reduced states observed in our simulations are essential for the functioning of the E-pathway. This suggestion should be the focus of future work that may possibly involve suitable mutagenesis experiments involving subtle alterations in the area lining the short water chain.

The minimum distances between the carboxyl groups of Glu-C/F180 and heme $b_D$ were shorter in the fully reduced states than in the fully oxidized states (Fig. 2, *e* and *f*). The semireduced state shows results similar to those of the fully reduced state. In the fully and semireduced states, the two carboxyl groups of Glu-180 and heme $b_D$ were sometimes as few as two hydrogen bonds from each other (0.4–0.6 nm). More precisely, the percentage of snapshots that have HBPs with length 2 is 1.1% of all the snapshots for path C, state B. For path F, it is 3.4% for state C, and 24.3% for state C′, (Fig. 3). In the fully oxidized states, however, those distances were much larger. These observations are correlated to the number of short HBPs found in each state. Apparently, the different distances resulted from the movement of Glu-C/F180 in the fully and semireduced states, because its all-atom RMSD (see Materials and Methods in the Supporting Material), as well as those of heme $b_D$, are much larger than those in the fully oxidized states (Fig. S10 and Fig. S11). These observations provide a clear structural explanation of why the E-pathway is only opened in the reduced state of this enzyme (where the distance between Glu-180 and heme $b_D$ is short; short HBPs are more populated, with only a few water molecules involved and much larger proton conductance) and not in the oxidized state (large distance between Glu-180 and heme $b_D$, almost no short HBPs, with more water molecules

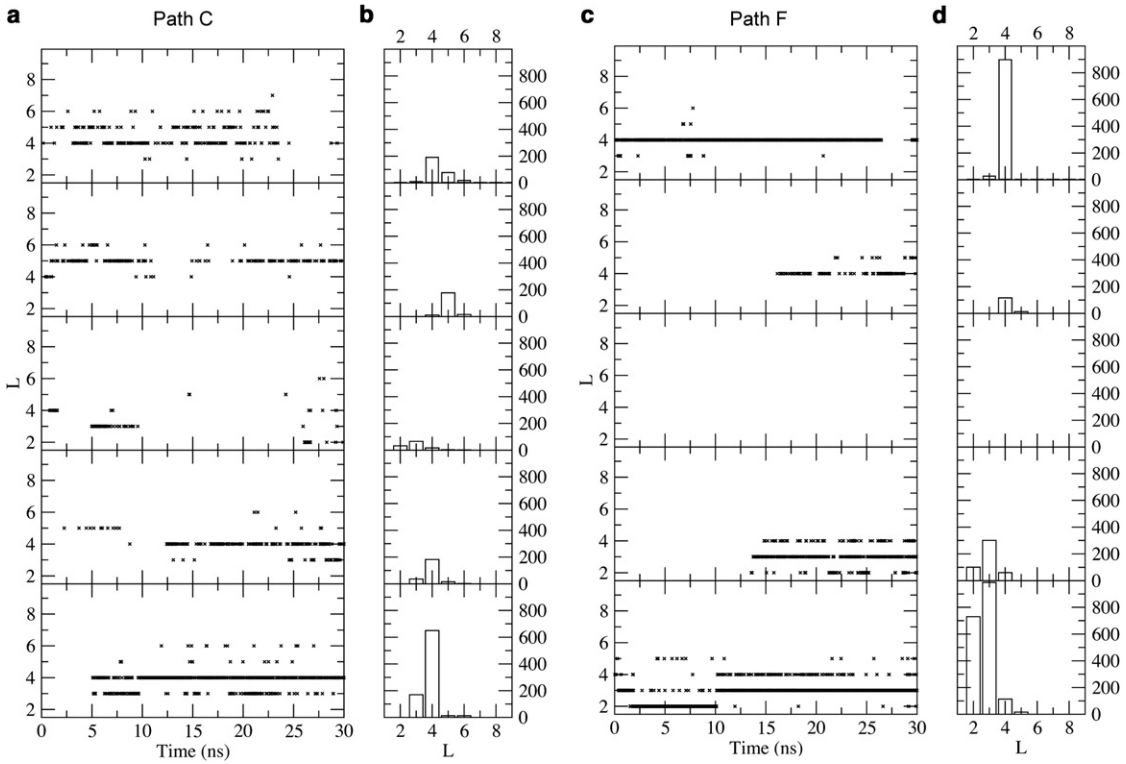


FIGURE 3 (*a*) Length of the connected hydrogen-bonding path between Glu-C180 and heme $b_D$ during the simulations. (*b*) Frequency of path lengths in *a*. (*c*) Length of the connected hydrogen-bonding path between Glu-F180 and heme $b_D$ during the simulations. (*d*) Frequency of path lengths in *c*. The path can contain as few as a single water molecule (two H-bonds). Data from top to bottom are for states A, A′, B, C, and C′.

involved and much smaller proton conductance). To achieve better statistics, a set of repeat runs of the same length was performed starting from different conformations. The results in these simulations were very similar to the first set of simulations (Fig. S12, Fig. S13, and Fig. S14). One might argue that if the actual proton-transfer pathway were to form only as a result of structural rearrangements that increase the probability of a cavity being hydrated, the MD simulations presented here would not identify it. However, we regard it as a merit of the MD simulations presented here that they require no large-scale conformational changes to explain the opening and closing of the investigated part of the E-pathway.

## Analyses of buried water molecules

To check whether the number of buried waters we added based on the GRID results influenced the result or not, we monitored the exchange of GRID waters and solvent waters between bulk solvent and a defined volume of the protein, as described in detail in the Supporting Material. In summary, we found (see Table S3 and Table S4) that water molecules exchanged frequently with the surrounding bulk solvent on a nanosecond timescale, so that it is unlikely that the number of water molecules inserted at the beginning of the simulation affect the final results.

## Involvement of His-44 in H-bond networks

In addition, we analyzed the hydrogen-bond networks involving His-C/F44. Similar to the analysis of Glu-C/F180, we first identified the HBPs between His-C/F44 and heme $b_D$ (using the H-bond definition given previously) and then computed the shortest length of each path (Fig. S15 and Fig. S16). Only in states A′ and C′ were a significant number of HBPs formed between His-C/F44 and heme $b_D$ (see Fig. S15, *Path C* and *Path F*, *right*). This indicates that in contrast to the HBPs between Glu-C/F180 and heme $b_D$, where the oxidation state plays a key role, the protonation state in this case appears to determine the formation of HBPs. In state A′, both path C and path F were enriched with HBPs, whereas in state C′, only path F was significantly enriched. This suggests that there might exist some asymmetry between the two monomers. It is also interesting that most of the HBPs in both states are of length 2 (with only one bridging water molecule). Results from the second set of simulations are consistent with these findings. When considering the HBPs between Glu-C/F180 and heme $b_D$ only in state C′, the HBPs between both Glu-C/F180 and heme $b_D$ and His-C/F44 and heme $b_D$ are enriched. A possible structural explanation for the formation of HBPs between His-C/F44 and heme $b_D$ is the rotation of the

side chain of His-C/F44 (Fig. 2 *d* and Fig. S17). These findings support the hypothesis (14) that His-C/F44 may serve an important role in forming a branching point to the E-pathway.

## Construction and properties of the strain *W. succinogenes* FrdC-H44E and the isolated His-C44 → Glu QFR variant enzyme

The mutant strain FrdC-H44E is compared in Table 1 to the wild-type and to the previously characterized strains FrdC-E66Q (8) and FrdC-E180Q (10), where the essential residues Glu-C66 (Fig. 1 *b*) at the menaquinol oxidation site and Glu-C180 at the heart of the E-pathway were replaced with a Gln. The mutants did not grow with fumarate as the terminal electron acceptor, but they did grow when nitrate (and brain-heart-infusion broth) replaced fumarate. As assayed with succinate oxidation by methylene blue, activities of the mutant cell homogenate and the isolated enzyme were roughly comparable to those of the wild-type. The activity monitored by this assay is independent of the diheme subunit C (61). However, when fumarate reductase activities were assayed by monitoring fumarate reduction by 2,3-dimethyl-1,4-naphthoquinol ($DMNH_2$), which is diheme-subunit-C-dependent (61), it was not detectable in the case of the membrane-bound variant enzymes. Upon solubilization of the isolated membranes with Triton X-100 (5,61,62), however, the activity of fumarate reduction by $DMNH_2$ for the E180Q variant was detectable and corresponded to approximately 1/10 that of the wild-type enzyme. In this respect, the E180Q variant differs significantly from the E66Q variant (8) and the H44E variant. Previous site-directed mutagenesis experiments (63) involving the replacement of His-C44 with Ala resulted in mutants with no fumarate reductase activity and no A or C subunits detectable by Western blotting and ELISA, indicating that the assembly of the enzyme complex requires proper heme ligation and underscoring the structural importance of the heme ligand His-C44. Consequently, analysis of the functional properties of His-C44 was not possible due to the lack of the H44A variant enzyme. Here, we have replaced His-C44 with a residue (Glu) that retains heme ligation properties, thus supporting assembly of the variant complex and thereby making possible the characterization of the H44E variant enzyme.

## Redox titration

A role of His-C44 in the proposed coupling of transmembrane proton transfer to transmembrane electron transfer via the heme groups should be reflected in a change of the oxidation-reduction midpoint potential, $E_M$, of at least one of the two heme groups upon replacement of His-C44 with Glu. Analysis of electrochemically induced absorbance difference spectra at wavelengths 428 nm (Soret band) and 561 nm ($\alpha$-band) for the variant and comparison to previously determined data for the wild-type and variant enzymes (see Fig. S18 and Table 1) indicated that this was indeed the case, as the midpoint potential, $E_M$, for the high-potential, proximal heme $b_P$ was decreased by almost 50 mV in the H44E variant, whereas that for the low-potential heme $b_D$ was lowered by ~30 mV. In this respect, the H44E variant differs significantly from the E66Q variant, which also lacks quinol oxidation activity but displays essentially unaltered heme $E_M$ values (8). It is unusual that the lowering of $E_M$ is apparently more pronounced for the heme ($b_P$) not affected directly by the ligand replacement, making it harder for $b_P$ to be reduced, most probably due to the lack of compensatory proton transfer from the quinol oxidation site to the E-pathway. These findings are fully consistent with

**TABLE 1 Growth and enzymatic activities of *W. succinogenes* FrdC-H44E cells and properties of the isolated QFR enzyme**

| | Strain wild-type | Strain FrdC-E66Q | Strain FrdC-E180Q | Strain FrdC-H44E |
|---|---|---|---|---|
| Growth with | | | | |
| formate + fumarate | + | — | — | — |
| formate + nitrate | + | + | + | + |
| Specific activity of membrane-bound enzyme in cell homogenate (U $mg^{-1}$ cell protein) | | | | |
| succinate → methylene blue | *0.31* | *0.17* | *0.35* | 0.25 |
| $DMNH_2$ → fumarate | *0.24* | *≤0.01* | *≤0.01* | ≤0.01 |
| Specific activity of isolated enzyme (U $mg^{-1}$ protein) | | | | |
| succinate → methylene blue | *28.8* | *16.9* | *24.9* | 3.78 |
| $DMNH_2$ → fumarate | *7.4* | *≤0.01* | *0.80* | ≤0.01 |
| Heme oxidation-reduction midpoint potentials $E_{M7}$ (mV) | | | | |
| Heme $b_P$ | *−10* | *−16* | *+39* | −57 |
| Heme $b_D$ | *−149* | *−145* | *−144* | −179 |

Values for wild-type, FrdC-E66Q (8), and FrdC-E180Q (10) are shown in italics for comparison. One unit (U) corresponds to 1 $\mu$mol of substrate turned over per minute.

the proposed role of His-C44 in the modified E-pathway hypothesis (Fig. 1).

## CONCLUSION

MD simulations were performed on five different redox states of the quinol:fumarate reductase. Analyses of the MD trajectories from the fully reduced state of the QFR with deprotonated $b_D$-C-propionate and protonated Glu-C180 strongly suggest that internal water molecules are involved in the transient proton transfer from the $b_D$-C-propionate to Glu-C180, the two important constituents identified experimentally in the E-pathway (10–13). Moreover, formation of configurations where proton transfer was likely to happen was correlated to the protonation state of the $b_D$-C-propionate. Short HBPs with high proton conductance from $b_D$-C-propionate to Glu-C/F180 were much more abundant in the fully reduced state of the QFR (states C and C′) than in the other three states. In contrast, in the fully oxidized or semireduced states, either no continuous H-bonded networks were formed in this region or the HBPs formed were mostly long paths that, it is postulated, can conduct protons at a much lower rate. This is in agreement with the experimental observation that in the fully oxidized state of the QFR, the E-pathway is blocked. Frequently formed short HBPs are essential for the functioning of the E-pathway. A structural characteristic of this opening/blocking transition is short minimum distances between the carboxyl groups of Glu-C/F180 and heme $b_D$ in the reduced states that facilitate the formation of short HBPs. A detailed analysis showed that transitions of these different distances resulted from the movement of the Glu-C/F180 side chains. In particular, the functional importance of the heme $b_D$-ligand His-C44 derived from the identification of hydrogen bonding paths between this side chain and the $b_D$-C-propionate provides a structural basis for the previously derived bifurcation of the E-pathway (14) (see also Fig. 1) and is consistent with the results from site-directed mutagenesis presented here.

## SUPPORTING MATERIAL

Seventeen figures, four tables, Supporting Materials and Methods, Supporting Results, and references (64–82) are available at http://www.biophysj.org/biophysj/supplemental/S0006-3495(12)00850-8.

NWChem Version 4.7, as developed and distributed by the Pacific Northwest National Laboratory (PNNL; P. O. Box 999, Richland, Washington 99352) and funded by the U. S. Department of Energy, was used for electronic structure calculations. We thank the Environmental Molecular Sciences Laboratory Grand Challenge Project (project gc20896) from PNNL for providing the computing resources. We thank Monica Sänger for valuable help with the initial mutagenesis experiments.

E.H. was supported by the International Max Planck Research School on Structure and Function of Biological Membranes. This work was supported by the Deutsche Forschungsgemeinschaft (SFB 472, the Cluster of Excellence Macromolecular Complexes, and grant He3875/9-1), the Max Planck Society, and Saarland University.

## REFERENCES

1. Kröger, A. 1978. Fumarate as terminal acceptor of phosphorylative electron transport. *Biochim. Biophys. Acta.* 505:129–145.
2. Lancaster, C. R. D. 2011. The superfamily of succinate:quinone oxidoreductases and its implications for the cyanobacterial enzymes. *In* Bioenergetic Processes of Cyanobacteria. G. A. Peschek, C. Obinger, and G. Renger, editors. Springer, Dordrecht, The Netherlands. 469–511.
3. Lancaster, C. R. D., and J. Simon. 2002. Succinate: quinone oxidoreductases from ε-proteobacteria. *Biochim. Biophys. Acta.* 1553:84–101.
4. Mileni, M., F. MacMillan, …, C. R. Lancaster. 2006. Heterologous production in *Wolinella succinogenes* and characterization of the quinol:fumarate reductase enzymes from *Helicobacter pylori* and *Campylobacter jejuni*. *Biochem. J.* 395:191–201.
5. Lancaster, C. R. D., A. Kröger, …, H. Michel. 1999. Structure of fumarate reductase from Wolinella succinogenes at 2.2 Å resolution. *Nature.* 402:377–385.
6. Madej, M. G., H. R. Nasiri, …, C. R. Lancaster. 2006. Evidence for transmembrane proton transfer in a dihaem-containing membrane protein complex. *EMBO J.* 25:4963–4970.
7. Lancaster, C. R. D., R. Gross, and J. Simon. 2001. A third crystal form of *Wolinella succinogenes* quinol:fumarate reductase reveals domain closure at the site of fumarate reduction. *Eur. J. Biochem.* 268:1820–1827.
8. Lancaster, C. R. D., R. Gross, …, A. Kröger. 2000. Essential role of Glu-C66 for menaquinol oxidation indicates transmembrane electrochemical potential generation by *Wolinella succinogenes* fumarate reductase. *Proc. Natl. Acad. Sci. USA.* 97:13051–13056.
9. Lancaster, C. R. D. 2002. *Wolinella succinogenes* quinol: fumarate reductase: 2.2-Å resolution crystal structure and the E-pathway hypothesis of coupled transmembrane proton and electron transfer. *Biochim. Biophys. Acta.* 1565:215–231.
10. Lancaster, C. R. D., U. S. Sauer, …, M. G. Madej. 2005. Experimental support for the "E pathway hypothesis" of coupled transmembrane $e^-$ and $H^+$ transfer in dihemic quinol:fumarate reductase. *Proc. Natl. Acad. Sci. USA.* 102:18860–18865.
11. Haas, A. H., and C. R. D. Lancaster. 2004. Calculated coupling of transmembrane electron and proton transfer in dihemic quinol:fumarate reductase. *Biophys. J.* 87:4298–4315.
12. Haas, A. H., U. S. Sauer, …, C. R. Lancaster. 2005. FTIR difference spectra of *Wolinella succinogenes* quinol:fumarate reductase support a key role of Glu-C180 within the "E-pathway hypothesis" of coupled transmembrane electron and proton transfer. *Biochemistry.* 44:13949–13961.
13. Mileni, M., A. H. Haas, …, C. R. Lancaster. 2005. Probing heme propionate involvement in transmembrane proton transfer coupled to electron transfer in dihemic quinol:fumarate reductase by $^{13}$C-labeling and FTIR difference spectroscopy. *Biochemistry.* 44:16718–16728.
14. Madej, M. G., F. G. Müller, …, C. R. D. Lancaster. 2009. Limited reversibility of transmembrane proton transfer assisting transmembrane electron transfer in a dihaem-containing succinate:quinone oxidoreductase. *Biochim. Biophys. Acta.* 1787:593–600.
15. Lancaster, C. R. D., E. Herzog, …, P. G. Schleidt. 2008. Electroneutral and electrogenic catalysis by dihaem-containing succinate:quinone oxidoreductases. *Biochem. Soc. Trans.* 36:996–1000.
16. Alder, B. J., and T. E. Wainwright. 1959. Studies in molecular dynamics. I. General method. *J. Chem. Phys.* 31:459–466.
17. McCammon, J. A., B. R. Gelin, and M. Karplus. 1977. Dynamics of folded proteins. *Nature.* 267:585–590.
18. Karplus, M., and J. A. McCammon. 2002. Molecular dynamics simulations of biomolecules. *Nat. Struct. Biol.* 9:646–652.

19. Friedman, R., E. Nachliel, and M. Gutman. 2005. Application of classical molecular dynamics for evaluation of proton transfer mechanism on a protein. *Biochim. Biophys. Acta.* 1710:67–77.

20. Voth, G. A. 2006. Computer simulation of proton solvation and transport in aqueous and biomolecular systems. *Acc. Chem. Res.* 39: 143–150.

21. Olkhova, E., M. C. Hutter, …, H. Michel. 2004. Dynamic water networks in cytochrome *c* oxidase from *Paracoccus denitrificans* investigated by molecular dynamics simulations. *Biophys. J.* 86:1873–1889.

22. Wikstrom, M., M. I. Verkhovsky, and G. Hummer. 2003. Water-gated mechanism of proton translocation by cytochrome c oxidase. *Biochim. Biophys. Acta.* 1604:61–65.

23. Kim, Y. C., M. Wikström, and G. Hummer. 2009. Kinetic gating of the proton pump in cytochrome *c* oxidase. *Proc. Natl. Acad. Sci. USA.* 106: 13707–13712.

24. Cukier, R. I. 2005. A molecular dynamics study of water chain formation in the proton-conducting K channel of cytochrome c oxidase. *Biochim. Biophys. Acta.* 1706:134–146.

25. Kandt, C., J. Schlitter, and K. Gerwert. 2004. Dynamics of water molecules in the bacteriorhodopsin trimer in explicit lipid/water environment. *Biophys. J.* 86:705–717.

26. Wolf, S., E. Freier, …, K. Gerwert. 2010. Directional proton transfer in membrane proteins achieved through protonated protein-bound water molecules: a proton diode. *Angew. Chem. Int. Ed. Engl.* 49:6889–6893.

27. Karplus, A. P., and C. Faerman. 1994. Ordered water in macromolecular structure. *Curr. Opin. Struct. Biol.* 4:770–776.

28. Carugo, O., and D. Bordo. 1999. How many water molecules can be detected by protein crystallography? *Acta Crystallogr. D Biol. Crystallogr.* 55:479–483.

29. Yu, B., M. Blaber, …, D. L. Caspar. 1999. Disordered water within a hydrophobic protein cavity visualized by X-ray crystallography. *Proc. Natl. Acad. Sci. USA.* 96:103–108.

30. Quillin, M. L., P. T. Wingfield, and B. W. Matthews. 2006. Determination of solvent content in cavities in IL-1$\beta$ using experimentally phased electron density. *Proc. Natl. Acad. Sci. USA.* 103:19749–19753.

31. Meyer, E. 1992. Internal water molecules and H-bonding in biological macromolecules: a review of structural features with functional implications. *Protein Sci.* 1:1543–1562.

32. Huang, Z., and E. Tajkhorshid. 2010. Identification of the third $Na^+$ site and the sequence of extracellular binding events in the glutamate transporter. *Biophys. J.* 99:1416–1425.

33. Holyoake, J., and M. S. P. Sansom. 2007. Conformational change in an MFS protein: MD simulations of LacY. *Structure.* 15:873–884.

34. Bakowies, D., and W. F. Van Gunsteren. 2002. Water in protein cavities: a procedure to identify internal water and exchange pathways and application to fatty acid-binding protein. *Proteins.* 47:534–545.

35. Lee, B., and F. M. Richards. 1971. The interpretation of protein structures: estimation of static accessibility. *J. Mol. Biol.* 55:379–400.

36. Richards, F. M. 1977. Areas, volumes, packing and protein structure. *Annu. Rev. Biophys. Bioeng.* 6:151–176.

37. Connolly, M. L. 1983. Analytical molecular surface calculation. *J. Appl. Cryst.* 16:548–558.

38. Helms, V. 2007. Protein dynamics tightly connected to the dynamics of surrounding and internal water molecules. *ChemPhysChem.* 8:23–33.

39. Goodford, P. J. 1985. A computational procedure for determining energetically favorable binding sites on biologically important macromolecules. *J. Med. Chem.* 28:849–857.

40. Helms, V., T. P. Straatsma, and J. A. McCammon. 1999. Internal dynamics of green fluorescent protein. *J. Phys. Chem. B.* 103:3263–3269.

41. Tara, S., V. Helms, …, J. A. McCammon. 1999. Molecular dynamics of mouse acetylcholinesterase complexed with huperzine A. *Biopolymers.* 50:347–359.

42. Dunitz, J. D. 1994. The entropic cost of bound water in crystals and biomolecules. *Science.* 264:670.

43. Zhang, L., and J. Hermans. 1996. Hydrophilicity of cavities in proteins. *Proteins.* 24:433–438.

44. Zheng, X. H., D. M. Medvedev, …, A. A. Stuchebrukhov. 2003. Computer simulation of water in cytochrome *c* oxidase. *Biochim. Biophys. Acta.* 1557:99–107.

45. Helms, V., and R. C. Wade. 1995. Thermodynamics of water mediating protein-ligand interactions in cytochrome P450cam: a molecular dynamics study. *Biophys. J.* 69:810–824.

46. Deng, Y., and B. Roux. 2008. Computation of binding free energy with molecular dynamics and grand canonical Monte Carlo simulations. *J. Chem. Phys.* 128:115103.

47. Helms, V., and R. C. Wade. 1998. Hydration energy landscape of the active site cavity in cytochrome P450cam. *Proteins.* 32:381–396.

48. Helms, V., and R. C. Wade. 1998. Computational alchemy to calculate absolute protein-ligand binding free energy. *J. Am. Chem. Soc.* 120:2710–2713.

49. Siu, S. W. I., R. Vácha, …, R. A. Böckmann. 2008. Biomolecular simulations of membranes: physical properties from different force fields. *J. Chem. Phys.* 128:125103.

50. Berendsen, H. J. C., J. R. Grigera, and T. P. Straatsma. 1987. The missing term in effective pair potentials. *J. Phys. Chem.* 91:6269–6271.

51. van der Spoel, D., R. van Drunen, and H. J. C. Berendsen. 1994. Groningen machine for chemical simulation. Groningen Machine for chemical simulation. Department of Biophysical Chemistry, BIOSON Research Institute, Nijenborgh 4 NL-9717 AG, Groningen, The Netherlands.

52. Cornell, W. D., P. Cieplak, …, P. A. Kollman. 1996. A second generation force field for the simulation of proteins, nucleic acids, and organic molecules (vol 117, pg 5179, 1995). *J. Am. Chem. Soc.* 118: 2309–2309.

53. Hess, B., H. Bekker, …, J. Fraaije. 1997. LINCS: A linear constraint solver for molecular simulations. *J. Comput. Chem.* 18:1463–1472.

54. Essmann, U., L. Perera, …, L. G. Pedersen. 1995. A smooth particle mesh Ewald method. *J. Chem. Phys.* 103:8577–8593.

55. Berendsen, H. J. C., J. P. M. Postma, …, J. R. Haak. 1984. Molecular dynamics with coupling to an external bath. *J. Chem. Phys.* 81:3684–3690.

56. Cox, M. J., R. L. A. Timmer, …, N. Agmon. 2009. Distance-dependent proton transfer along water wires connecting acid-base pairs. *J. Phys. Chem. A.* 113:6599–6606.

57. Siwick, B. J., and H. J. Bakker. 2007. On the role of water in intermolecular proton-transfer reactions. *J. Am. Chem. Soc.* 129:13412–13420.

58. Siwick, B. J., M. J. Cox, and H. J. Bakker. 2008. Long-range proton transfer in aqueous acid-base reactions. *J. Phys. Chem. B.* 112:378–389.

59. Gu, W., and V. Helms. 2009. Tightly connected water wires facilitate fast proton uptake at the proton entrance of proton pumping proteins. *J. Am. Chem. Soc.* 131:2080–2081.

60. Grossfield, A., and D. M. Zuckerman. 2009. Quantifying uncertainty and sampling quality in biomolecular simulations. *In* Annual Reports in Computational Chemistry. A. W. Ralph, editor. Elsevier, New York. 23–48.

61. Unden, G., H. Hackenberg, and A. Kröger. 1980. Isolation and functional aspects of the fumarate reductase involved in the phosphorylative electron transport of *Vibrio succinogenes*. *Biochim. Biophys. Acta.* 591:275–288.

62. Lancaster, C. R. D. 2003. Crystallization of *Wolinella succinogenes* quinol:fumarate reductase. *In* Membrane Protein Purification and Crystallization: A Practical Guide, 2nd ed.. C. Hunte, H. Schägger, and G. von Jagow, editors. Academic Press, San Diego. 219–228.

63. Simon, J., R. Gross, …, A. Kröger. 1998. Deletion and site-directed mutagenesis of the *Wolinella succinogenes* fumarate reductase operon. *Eur. J. Biochem.* 251:418–426.

64. Juhnke, H. D., H. Hiltscher, …, C. R. Lancaster. 2009. Production, characterization and determination of the real catalytic properties of

the putative "succinate dehydrogenase" from *Wolinella succinogenes*. *Mol. Microbiol.* 71:1088–1101.

65. Bronder, M., H. Mell, …, A. Kröger. 1982. Biosynthetic pathways of *Vibrio succinogenes* growing with fumarate as terminal electron acceptor and sole carbon source. *Arch. Microbiol.* 131:216–223.
66. Lorenzen, J. P., A. Kröger, and G. Unden. 1993. Regulation of the anaerobic respiratory pathways in *Wolinella succinogenes* by the presence of electron acceptors. *Arch. Microbiol.* 159:477–483.
67. Bode, C., H. Goebell, and E. Stähler. 1968. Elimination of errors caused by turbidity in the determination of protein by the biuret method. *Z. Klin. Chem. Klin. Biochem.* 6:418–422.
68. Reference deleted in proof.
69. Unden, G., and A. Kröger. 1981. The function of the subunits of the fumarate reductase complex of *Vibrio succinogenes*. *Eur. J. Biochem.* 120:577–584.
70. Mäntele, W. 1996. Infrared and Fourier transform infrared spectroscopy. *In* Biophysical Techniques in Photosynthesis. A. J. Hoff and J. Amesz, editors. Kluwer, Dordrecht, The Netherlands. 137–160.
71. Moss, D., E. Nabedryk, …, W. Mäntele. 1990. Redox-linked conformational changes in proteins detected by a combination of infrared spectroscopy and protein electrochemistry. Evaluation of the technique with cytochrome *c*. *Eur. J. Biochem.* 187:565–572.
72. Mäntele, W. 1993. Reaction-induced infrared difference spectroscopy for the study of protein function and reaction mechanisms. *Trends Biochem. Sci.* 18:197–202.
73. Baymann, F., D. A. Moss, and W. Mäntele. 1991. An electrochemical assay for the characterization of redox proteins from biological electron transfer chains. *Anal. Biochem.* 199:269–274.
74. Lancaster, C. R. D., and H. Michel. 1997. The coupling of light-induced electron transfer and proton uptake as derived from crystal structures of reaction centres from *Rhodopseudomonas viridis* modified at the binding site of the secondary quinone, $Q_B$. *Structure.* 5:1339–1359.
75. Kendall, R. A., E. Apra, …, A. T. Wong. 2000. High performance computational chemistry: an overview of NWChem a distributed parallel application. *Comput. Phys. Commun.* 128:260–283.
76. Faraldo-Gómez, J. D., G. R. Smith, and M. S. P. Sansom. 2002. Setting up and optimization of membrane protein simulations. *Eur. Biophys. J.* 31:217–227.
77. Hub, J. S., F. K. Winkler, …, B. L. de Groot. 2010. Potentials of mean force and permeabilities for carbon dioxide, ammonia, and water flux across a *Rhesus* protein channel and lipid membranes. *J. Am. Chem. Soc.* 132:13251–13263.
78. Susankova, K., R. Ettrich, …, V. Vlachova. 2007. Contribution of the putative inner-pore region to the gating of the transient receptor potential vanilloid subtype 1 channel (TRPV1). *J. Neurosci.* 27:7578–7585.
79. Giachetti, A., G. L. La Penna, …, L. Banci. 2004. Modeling the backbone dynamics of reduced and oxidized solvated rat microsomal cytochrome $b_5$. *Biophys. J.* 87:498–512.
80. Weiner, S. J., P. A. Kollman, …, P. Weiner. 1984. A new force field for molecular mechanical simulation of nucleic acids and proteins. *J. Am. Chem. Soc.* 106:765–784.
81. Cornell, W. D., P. Cieplak, …, P. A. Kollman. 1995. A second generation force field for the simulation of proteins, nucleic acids, and organic molecules. *J. Am. Chem. Soc.* 117:5179–5197.
82. Lancaster, C. R. D., A. H. Haas, …, M. Mileni. 2006. Recent progress on obtaining theoretical and experimental support for the "E-pathway hypothesis" of coupled transmembrane electron and proton transfer in dihaem-containing quinol: fumarate reductase. *Biochim. Biophys. Acta.* 1757:988–995.